Dynamical (e, 2e) studies of formic acid

2009 J. Phys. B: At. Mol. Opt. Phys. 42 235207

(http://iopscience.iop.org/0953-4075/42/23/235207)

J. Phys. B: At. Mol. Opt. Phys. **42** (2009) 235207 (6pp) doi:10.1088/0953-4075/42/23/235207

Dynamical (e, 2e) studies of formic acid

C J Colyer[1], M A Stevenson[1], O Al-Hagan[2], D H Madison[2], C G Ning[3] and B Lohmann[1]

[1] ARC Centre of Excellence for Antimatter-Matter Studies, The University of Adelaide, Adelaide, SA 5005, Australia
[2] Department of Physics, Missouri University of Science and Technology, Rolla, MO 65409, USA
[3] Department of Physics and Key Laboratory of Atomic and Molecular NanoSciences of MOE, Tsinghua University, Beijing 100084, People's Republic of China

Received 7 September 2009, in final form 21 October 2009
Published 23 November 2009
Online at stacks.iop.org/JPhysB/42/235207

Abstract
We present triply differential cross sections for the electron impact ionization of the outer valence orbitals of formic acid (CHOOH) by 100 eV and 250 eV incident electrons. The experiments were performed under asymmetric kinematics, in which the outgoing ejected electron had an energy of 10 eV, over a range of momentum transfers. The experimental results are compared with theoretical calculations carried out using the sophisticated M3DW model, both with and without correlation-polarization-exchange terms included.

(Some figures in this article are in colour only in the electronic version)

1. Introduction

Electron impact ionization is a fundamental process which is important in a wide range of physical phenomena. The most complete information about this process is obtained by detecting the incident electron, after it has been scattered by the ionization event, and the electron ejected from the target, in time coincidence (the (e, 2e) technique). If the energies and momenta of the incident and outgoing electrons are all specified, this yields a measure of the triple differential cross section (TDCS). The study of electron impact ionization of atomic targets using this technique can be considered a mature field [1]; however, this is not the case for molecular targets. The experimental difficulties associated with TDCS measurements for molecular targets arise from the limits on the ability of the experiment to resolve different molecular orbitals which can, depending on the molecular configuration of the target, be quite closely spaced in energy. Nevertheless, TDCS measurements which probe the dynamics of the collision process are available for a number of molecules ranging from simple diatomics such as H_2 [2–5] and N_2 [6–8] to more complicated molecules such as H_2O [9, 10], CO_2 [11], C_2H_2 [12] and N_2O [13]. Electron momentum spectroscopy (EMS) studies which use the coincidence technique to obtain structure information are more numerous, and extend to more complex molecules [14].

There is considerable interest in the dynamics of the ionization process in interactions of ionizing radiation with biological matter. In the last decade, experimental studies have indicated that secondary particles produced by the primary ionizing particle can play a significant role in radiation damage to DNA [15]. In the ionization process, large numbers of secondary electrons with comparatively low energies (0–20 eV) are liberated, which then interact with biomolecules such as sugars [16, 17], water [18], and the DNA and RNA bases [19–21]. Water in particular has recently been the focus of several theoretical [22–24] and experimental [9, 10] dynamical (e, 2e) investigations, with a view to quantifying the interaction of electrons with biological matter using water as an approximation for living tissue. The primary focus of the present study is to further understand this electronic interaction using smaller biomolecules, such as formic acid, as a model for the components of larger biological systems.

Most famously known for its role in the venom of ants and bees, formic acid is the simplest organic acid and is thought to play a key role in the formation of larger biologically relevant molecules, such as acetic acid and glycine. It was detected in the interstellar medium [25] and constitutes, together with glycine, one of the simplest building blocks of more complicated biological systems [26]. To date, the majority of experimental studies of this molecule involving electron impact have been of dissociative electron attachment [27–29], while elastic and vibrationally inelastic differential scattering measurements have appeared more recently [30, 31]. The structure of formic acid has been rigorously probed by three EMS studies [32–34] where the latter study constituted the first

EMS study of the formic acid monomer without contributions from the dimer. To the authors' best knowledge, no dynamical studies exist for formic acid.

In this paper, we present measurements of the TDCS for electron impact ionization of gas phase formic acid molecules. We compare the experimental results with distorted wave calculations of the TDCS. Where possible, the experimental data are also compared to the previous experiments performed on water by Milne-Brownlie *et al* [9] under the same kinematics.

2. Experimental apparatus

This study has been conducted in a conventional (e, 2e) spectrometer, operating in the coplanar asymmetric geometry. The apparatus has been described in detail previously [35]. Briefly, the spectrometer consists of an electron gun and two hemispherical electron energy analysers, all mounted in-plane and perpendicular to the target gas jet. The electron gun consists of six cylindrical electrostatic lens elements, incorporating a thoriated tungsten filament as the source, with a resultant electron beam energy width of approximately 0.5 eV FWHM. The hemispherical analysers are preceded by five cylindrical electrostatic lens elements and are mounted on independently rotatable turntables, concentric with the interaction region. Electrons exiting the analysers are detected by channel electron multipliers and, via the use of fast-timing electronics, can be determined to originate from the same event. The coincidence energy resolution of the system is approximately 1.2 eV FWHM.

The formic acid vapour target enters the interaction region via a 0.69 mm stainless steel capillary. The vapour is obtained from a liquid sample held in a glass vial, of 98% stated purity (Sigma-Aldrich, Australia), and further purified via several freeze-pump-thaw cycles. The vapour is a mixture of monomers and dimers whose ratio is a function of temperature and driving pressure. At higher temperatures, the extra kinetic energy serves to break up most of the dimers into monomers. It was demonstrated in [33] that at temperatures in excess of 120 °C, the target is composed of greater than 99% monomers. As a result, the beam-forming needle is held at approximately 135 °C, while the associated gas handling system and vacuum chamber are heated to approximately 75 °C and 50 °C respectively to prevent condensation.

In asymmetric kinematics, the fast outgoing electron is usually referred to as the scattered electron whilst the slow outgoing electron is termed the ejected electron. This geometry implies that the scattered electron energy analyser be held at a fixed forward angle while the ejected electron energy analyser is rotated in the scattering plane. Also, the scattered electron energy E_a is generally much larger than the ejected electron energy E_b. Through energy conservation the incident electron energy can be determined:

$$E_0 = E_a + E_b + \varepsilon_i, \tag{1}$$

where E_0 is the incident electron energy and ε_i is the binding energy of the orbital in question. From conservation of momentum the recoil ion momentum, $\mathbf{p}$, can be obtained:

$$\mathbf{p} = \mathbf{k}_0 - \mathbf{k}_a - \mathbf{k}_b, \tag{2}$$

where $\mathbf{k}_0$ is the incident electron momentum, $\mathbf{k}_a$ is the scattered electron momentum and $\mathbf{k}_b$ is the ejected electron momentum.

The momentum transferred to the target, $\mathbf{K}$, can then be defined as

$$\mathbf{K} = \mathbf{k}_0 - \mathbf{k}_a. \tag{3}$$

3. Theory

The details of the molecular three-body distorted wave (M3DW) approximation have been presented elsewhere [36–38], so only a brief overview will be presented here. The M3DW TDCS is given by

$$\frac{\mathrm{d}^5\sigma}{\mathrm{d}\Omega_a\,\mathrm{d}\Omega_b\,\mathrm{d}E_b} = \frac{1}{(2\pi)^5}\frac{k_a k_b}{k_i}(|T_{\mathrm{dir}}|^2 + |T_{\mathrm{exc}}|^2 + |T_{\mathrm{dir}} - T_{\mathrm{exc}}|^2), \tag{4}$$

where $\vec{k}_i$ is the initial-state wave vector, $\vec{k}_a$ ($\vec{k}_b$) is the wave vector for the scattered (ejected) electron and the direct and exchange amplitudes are T_{dir} and T_{exc} respectively:

$$T_{\mathrm{dir}} = \langle \chi_a^-(\vec{k}_a, \mathbf{r}_1)\chi_b^-(\vec{k}_b, \mathbf{r}_2)C_{\mathrm{scat-eject}}(r_{12}) \times |V - U_i|\phi_j^{\mathrm{OA}}(\mathbf{r}_2)\chi_i^+(\vec{k}_i, \mathbf{r}_1)\rangle \tag{5}$$

$$T_{\mathrm{exc}} = \langle \chi_a^-(\vec{k}_a, \mathbf{r}_2)\chi_b^-(\vec{k}_b, \mathbf{r}_1)C_{\mathrm{scat-eject}}(r_{12}) \times |V - U_i|\phi_j^{\mathrm{OA}}(\mathbf{r}_2)\chi_i^+(\vec{k}_i, \mathbf{r}_1)\rangle. \tag{6}$$

In equations (5) and (6), $\mathbf{r}_1(\mathbf{r}_2)$ is the coordinate of the incident (bound) electron, χ_i, χ_a and χ_b are the distorted waves for the incident, scattered and ejected electrons, respectively, $C_{\mathrm{scat-eject}}$ is the Coulomb interaction between the scattered projectile and ejected electron and ϕ_j^{OA} is the orientation-averaged molecular orbital (OAMO) [36] for the initial bound state wavefunction of the molecule generated from molecular orbitals. The molecular wavefunction was calculated using density functional theory (DFT) along with the standard hybrid B3LYP [39] functional by means of the ADF 2007 (Amsterdam density functional) program [40] with the TZ2P (triple-zeta with two polarization functions) Slater-type basis sets. In the next section, experimental results will be shown for the sum of the 10a′ and 2a″ valence orbitals of formic acid. Unfortunately the OAMO approximation is not valid for the 2a″ orbital since the average is zero for this symmetry. Consequently, we are able to calculate results for the 10a′ orbital only. The potential V is the initial-state interaction between the projectile and the neutral molecule, and U_i is the initial-state spherically symmetric distorting potential which is used to calculate the initial-state distorted wave χ_i.

The initial-state molecular distorted waves are calculated using a spherically symmetric distorting potential U_i. The Schrödinger equation for the incoming electron wavefunction is given by

$$\left(T + U_i - \frac{k_i^2}{2}\right)\chi_i^+(\vec{k}_i, \boldsymbol{r}) = 0, \tag{7}$$

where T is the kinetic energy operator, and the '+' superscript on $\chi_i^+(\vec{k}_i, \boldsymbol{r})$ indicates outgoing wave boundary conditions. The initial-state distorting potential contains three components

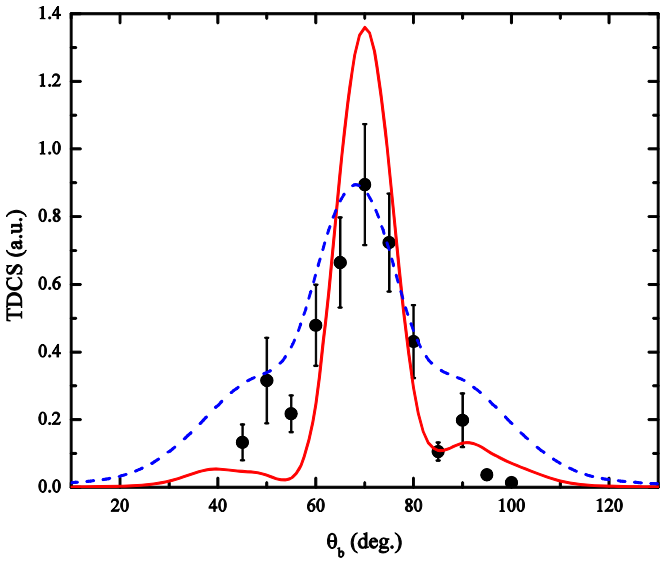

Figure 1. Experimental triple differential cross section for the 10a′ valence orbital of formic acid (solid circles) as a function of ejected electron scattering angle, compared with M3DW-CPE (solid line) and PWIA (dashed line) calculations. The incident electron energy is 831.6 eV, the projectile scattering angle is 20.5°, and the ejected electron energy is 105 eV. The experimental data and the PWIA results are those of Nixon *et al* [34].

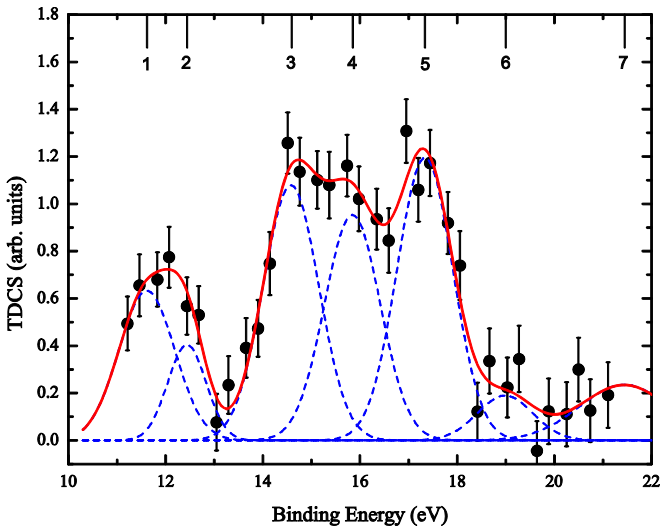

Figure 2. Measured binding energy spectrum for the outer valence orbital region of formic acid, fitted with a sum of Gaussian functions.

$U_i = U_S + U_E + U_{CP}$, where U_S is the initial-state spherically symmetric static potential which is calculated from the molecular charge density obtained from the numerical orbitals averaged over all angular orientations, U_E is the exchange-distortion potential of Furness and McCarthy [41] and U_{CP} is the correlation-polarization potential of Perdew and Zunger [42] (see also Padial and Norcross [43]).

The two final channel distorted waves are obtained from a Schrödinger equation similar to equation (7):

$$\left(T + U_f - \frac{k_{a(b)}^2}{2}\right) \chi_{a(b)}^{-}(\vec{k}_{a(b)}, \boldsymbol{r}) = 0. \tag{8}$$

Here $U_f = U_I + U_E + U_{CP}$, where U_I is the final-state spherically symmetric static distorting potential for the molecular ion which is calculated using the same procedure as for U_S except that the active electron is removed from the charge distribution. Two calculations have been performed—one excluding $U_E + U_{CP}$ which we label M3DW and one including $U_E + U_{CP}$ which we label M3DW-CPE.

An idea of the quality of our OAMO wavefunction can be achieved by comparing theory and experiment at higher incident electron energies where kinematics will play a minor role. Nixon *et al* [34] reported an EMS study of formic acid which differentiated between the 10a′ and 2a″ orbitals for an incident electron energy of 831.6 eV. Figure 1 compares the present M3DW-CPE results with the Nixon *et al* [34] measurements and the theoretical PWIA (plane wave impulse approximation) results reported in the paper. In the PWIA, the cross section is directly proportional to the square of the molecular wavefunction averaged over all orientations. The PWIA calculation used the B3LYP/TZVP molecular wavefunction [34] while we used B3LYP/TZ2P. It was checked that these two different wavefunctions produced essentially identical results when used in the M3DW-CPE calculation. Whereas we use the OAMO approximation, the PWIA performs a proper average over molecular orientations without making approximations. Consequently, the difference between the two theoretical curves in figure 1 represents the effects of the OAMO approximation plus the difference between using the plane wave impulse approximation and the distorted wave Born approximation (DWBA). Arguably, the M3DW-CPE results are in better overall agreement with the experimental data which would be understandable from the point of view that if kinematics are important, the DWBA should be better than the PWIA and 800 eV is low enough an energy that kinematics might start playing a role. However, for this to be true, the OAMO approximation would also have to be valid. Consequently, the good agreement between the M3DW-CPE and the high-energy experiment shown in figure 1 indicates that the OAMO approximation is reasonably good for the 10a′ state.

4. Results and discussion

The experiments were performed at two incident electron energies: a lower value of 100 eV and a higher value of 250 eV. In both cases the ejected electron energy was chosen to be 10 eV. Figure 2 shows a coincidence binding energy spectrum of the outer valence region of formic acid, where the incident and ejected electron energies are fixed at 250 eV and 10 eV, respectively, while the scattered electron energy is scanned across a range of energies. The detection angles for the scattered and ejected electrons were chosen to be −5° and 90° respectively. This sets the ejected electron detection angle 30° larger than the momentum transfer direction so that contributions from both s-type and p-type orbitals would be evident. The outer valence region of formic acid consists of seven molecular orbitals: five in the molecular plane (a′) and two out of the molecular plane (a″) [32]. All seven orbitals can

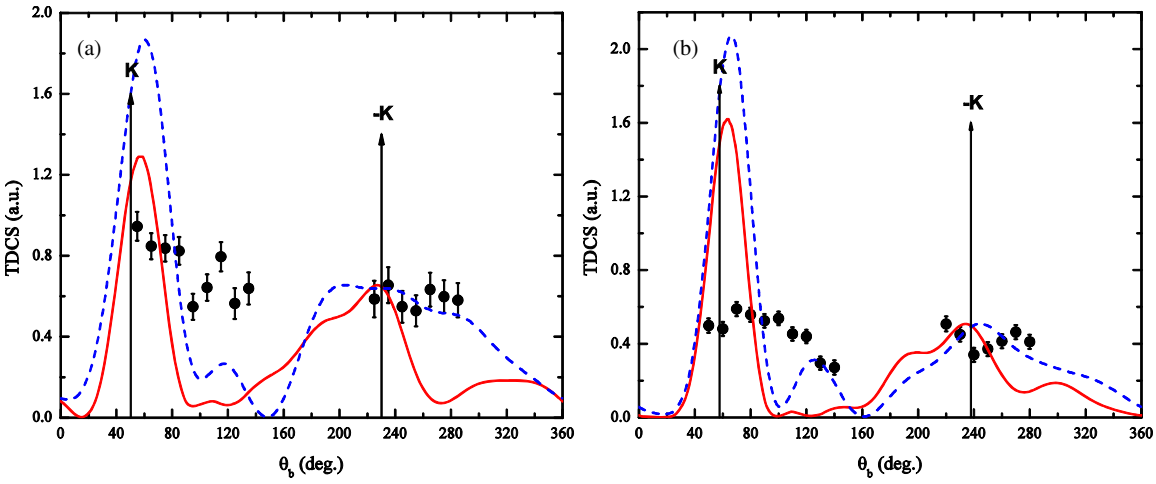

Figure 3. Experimental triple differential cross sections for the summed 10a′ and 2a″ valence orbitals of formic acid (solid circles), with $E_0 = 100$ eV and $E_b = 10$ eV, compared with M3DW-CPE (solid line) and M3DW (dashed line) calculations for the 10a′ orbital only. The scattered electron detection angles and corresponding momentum transfers are (a) -10°, $|K| = 0.54$ au and (b) -15°, $|K| = 0.74$ au.

be partially resolved; however, due to the limited coincident energy resolution of the apparatus and the intensity of each orbital under the chosen kinematics, not all orbitals can be completely separated. Table 1 shows the binding energy of each orbital, as well as the assignments and energies as determined via EMS [33] and photoelectron spectroscopy (PES) [44]. Here we present angular distributions for the summed outermost valence orbitals (10a′ + 2a″). Examination of the momentum density probability distributions for the 10a′ and 2a″ orbitals presented in [32] indicates that, for all scattering angles considered here, one may expect the contribution of the 10a′ orbital to be considerably larger than that of the 2a″ orbital at ejected electron angles around 60° and the contributions to be approximately equal at angles around 120°.

Figures 3(a) and (b) show the experimental results for the summed 10a′ and 2a″ orbitals, compared to theoretical results for the 10a′ orbital only for the TDCS of the formic acid monomer at an incident energy of 100 eV and an ejected electron energy of 10 eV, for scattered electron angles of -10° and -15° respectively. The angular distributions can be divided into two regions, the binary region ranging from 0° to 180° and the recoil region which ranges from 180° to 360°. The binary region is so named because the structure here arises from single binary collisions. Depending upon the kinematics, the TDCS in the binary region may contain strong signatures of the orbital structure [45]. In contrast, the recoil structure arises from processes whereby the ejected electron produced by an initial binary collision undergoes subsequent recoil scattering from the target nucleus. As the experimental data are not on an absolute scale, they have been normalized to the M3DW-CPE calculation so as to give the best visual fit in the recoil region. We have used the recoil region for the normalization since, from the work of Bharathi *et al* [32], it is known that the shape and width of the binary peak will be strongly affected by the 2a′ state, which is not included in the theory. It is evident from the relative size of the peaks in the binary and recoil regions that a large amount of interaction between the ejected electron and the target nucleus is present at these energies. The M3DW and M3DW-CPE calculations achieve reasonable qualitative agreement with the experimental results in figures 3(a) and (b), but tend to predict a larger and sharper binary peak than is observed in the experiment. The simpler M3DW agrees well with the shape of the recoil peak; the addition of the CPE terms improves the binary peak to recoil peak ratio but appears to worsen the shape agreement in the recoil region. However, since the theoretical calculation is for the 10a′ orbital only while the experiment is summed 10a′ + 2a″, it is difficult to evaluate the accuracy of the theory. For example, the fact that the M3DW gives the best agreement with the shape of the recoil peak may be fortuitous since it is quite possible that the M3DW-CPE gives the correct shape and the additional width of the peak comes from the 2a″ orbital. The additional experimental structure in the binary peak for angles between 90° and 120° very likely originates from the 2a″ orbital. Although the details of the cross section will undoubtedly be different for our kinematics, we believe that this proposition is again supported by an examination of the momentum density profiles reported by Bharathi *et al* [32]. Plotting their momentum profiles against ejected electron angle, and summing the profiles, indicates that the resultant cross section is enhanced in the region from 90° to 120°, compared with the cross section for only the 10a′ orbital.

Figures 4(a)–(c) present the TDCS for electron impact ionization of formic acid with 250 eV incident electrons,

Table 1. Formic acid binding energies (in eV), with the error in the Gaussian peak position quoted in parentheses.

	Orbital	Present results	EMS [33]	PES [44]
1	10a′	11.6 (6)	11.5	11.5
2	2a″	12.5 (4)	12.65	12.6
3	9a′	14.6 (6)	14.7	14.8
4	1a″	15.8 (6)	15.8	15.8
5	8a′	17.3 (6)	17.15	17.1
6	7a′	19.0 (6)	17.9	17.8
7	6a′	21.5 (9)	22	22

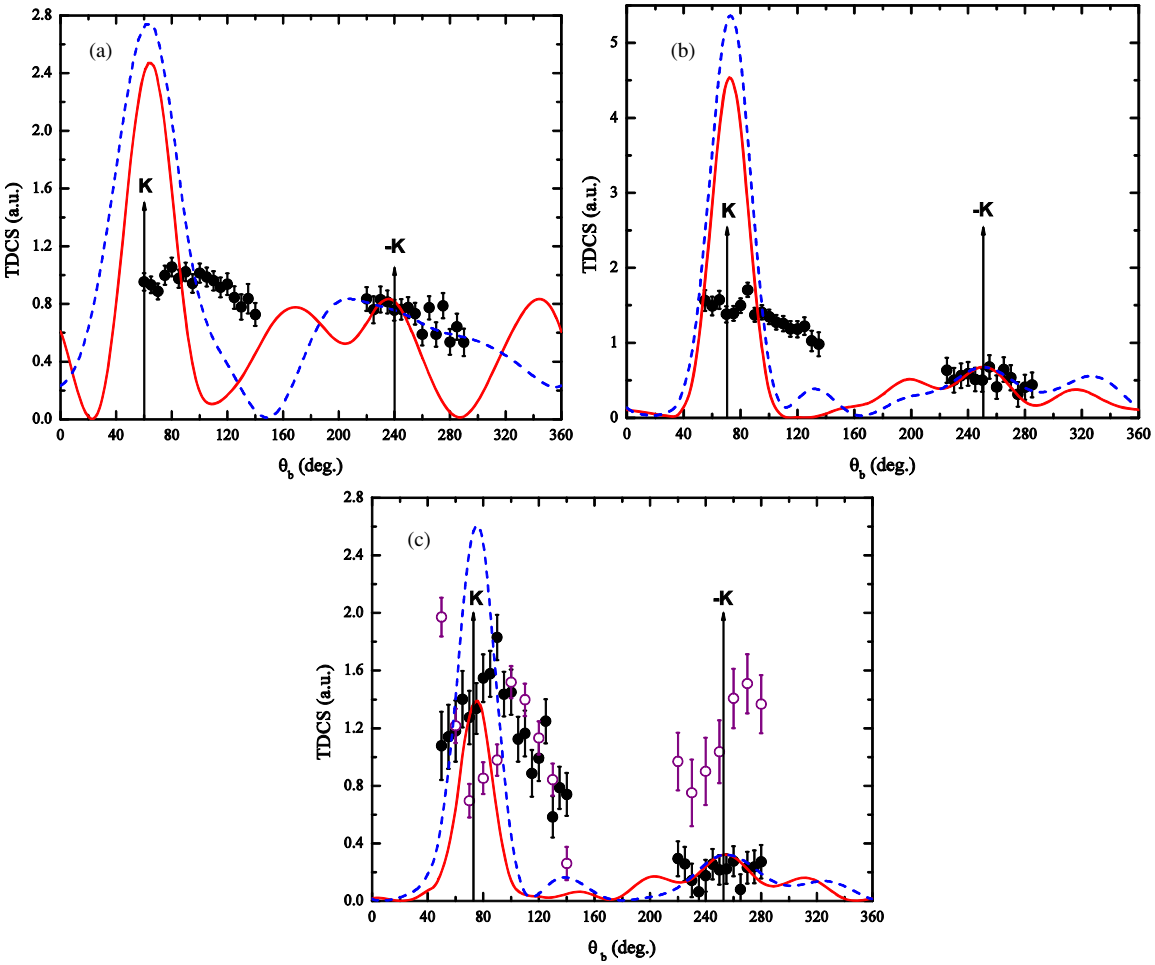

Figure 4. Experimental triple differential cross sections for the summed 10a′ and 2a″ valence orbitals of formic acid (solid circles), with $E_0 = 250$ eV and $E_b = 10$ eV, plotted against the M3DW-CPE (solid line) and M3DW (dashed line) calculations for the 10a′ orbital only (a, b). Panel (c) includes previous experimental results for the summed $3a_1 + 1b_1$ orbitals for water under the same kinematics [9] (open circles). The scattered electron detection angles and corresponding momentum transfers are (a) $-5°$, $|K| = 0.42$ au, (b) $-10°$, $|K| = 0.75$ au and (c) $-15°$, $|K| = 1.11$ au.

measured for 10 eV ejected electrons. Results are presented for three scattering angles: (a) $-5°$ (b) $-10°$ and (c) $-15°$. Results for the experimentally determined TDCS for ionization of the summed $1b_1 + 3a_1$ valence orbitals for H_2O [9] under the same kinematics as in figure 4(c) are also presented in that figure. Immediately clear is the difference in the relative size of the binary and recoil peaks at an incident energy of 250 eV when compared to the lower energy case. As the scattered electron angle changes from $-5°$ to $-10°$ to $-15°$, the magnitude of the recoil peak relative to the binary peak decreases significantly, in contrast to the case in figure 3, where the binary/recoil ratio is approximately constant as the scattering angle is changed from $-10°$ to $-15°$. The relative magnitude of the recoil peak compared to the binary peak at a scattering angle of $-15°$ (figure 4) is in stark contrast to the data from [9] for H_2O, which under the same conditions produces a recoil peak approximately four times greater. In a recent study [46], out of plane TDCS measurements for H_2 and He were compared, and through the use of state-of-the-art theory, certain structures were determined to arise from recoil interactions; the magnitude of these structures could be increased by minimizing the internuclear separation of H_2 to the extent that it represents the localized single-centre nuclear charge of helium. In light of this, it seems reasonable to suggest that this lack of recoil interaction in formic acid may be attributed to the molecule's polycentric nature, and thus the lack of nuclear charge at the centre of mass, as opposed to the water molecule which has a single oxygen nucleus at its centre (see figure 5). In comparison with the theoretical calculations, the M3DW again predicts quite well the shape of the recoil peaks in all cases, and there is also improved agreement with the M3DW-CPE in this region, especially at the larger momentum transfers. The relative size of the binary and recoil peaks is still predicted better by the M3DW-CPE, but both calculations still do not predict the size and shape of the binary peak, except in figure 3(c), where the M3DW-CPE successfully predicts the correct relative magnitudes of the binary peak and the recoil peak, and the sharper binary peak observed at this larger momentum transfer more closely resembles the peak predicted by the calculation. The sharper binary peak for these kinematics made is indicative of a smaller contribution from the 2a″ orbital.

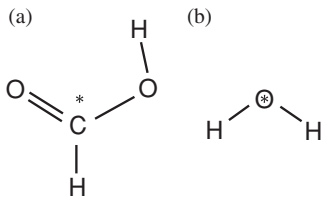

Figure 5. Molecular structures of (a) formic acid and (b) water. The centre of mass for each molecule is marked by an asterisk.

5. Conclusions

The present paper constitutes the first dynamical (e, 2e) study for the formic acid molecule. The measured binding energies and orbital assignments are in good agreement with the available EMS and PES data. Experimental cross sections for the formic acid monomer exhibit a significant change in binary peak shape as the scattering angle is varied, and a ratio between the recoil peak magnitude and binary peak magnitude which is much smaller than that observed for ionization of water under the same kinematics. The theoretical calculations for the 10a′ state exhibit very good agreement with EMS cross sections measured for higher incident electron energies. This indicates that the OAMO approximation is reasonably good for this state. However, the agreement between theory and the present experimental results summed over the 10a′ and 2a′′ states is not very good, particularly in the binary region, and this is most likely due to the 2a′′ contribution. The M3DW results are in reasonable agreement with the summed experimental cross sections in the recoil region which seems odd since the M3DW-CPE would be expected to be better. However, this may be fortuitous again due to the 2a′′ contribution. Reasonable agreement between experiment and theory was found for the higher incident energy and largest scattering angle which suggests that the 2a′′ contribution might be small for this case. This is the first time that the M3DW method has been applied to a large molecule such as this. We are encouraged by the good agreement that was found with the 10a′ EMS measurements, and the opportunity to compare the performance of these calculations would be enhanced by further experimental data for the individual, as opposed to summed orbitals.

Acknowledgments

This work was supported by the Australian Research Council Centre of Excellence for Antimatter-Matter Studies and the American NSF under grant number 0757749. The author CGN would like to acknowledge the support of the National Natural Science Foundation of China under contract no 10704046, and the author OA-H would like to acknowledge the support of the Saudi Ministry of Higher Education's King Abdullah Bin Abdul-Aziz Scholarship. The authors are grateful to K Nixon for providing the EMS data in numerical form.

References

[1] Lahmam-Bennani A 1991 *J. Phys. B: At. Mol. Opt. Phys.* **24** 2401
[2] Jung K *et al* 1975 *J. Phys. B: At. Mol. Opt. Phys.* **8** 1330
[3] Cherid M *et al* 1989 *J. Phys. B: At. Mol. Opt. Phys.* **22** 3483
[4] Milne-Brownlie D S *et al* 2006 *Phys. Rev. Lett.* **96** 233201
[5] Gao J *et al* 2006 *J. Chem. Phys.* **124** 194306
[6] Avaldi L *et al* 1992 *J. Phys. B: At. Mol. Opt. Phys.* **25** 3551
[7] Murray A J *et al* 2006 *J. Phys. B: At. Mol. Opt. Phys.* **39** 3945
[8] Naja A *et al* 2007 *J. Phys. B: At. Mol. Opt. Phys.* **40** 3775
[9] Milne-Brownlie D S *et al* 2004 *Phys. Rev.* A **69** 032701
[10] Kaiser C *et al* 2007 *J. Phys. B: At. Mol. Opt. Phys.* **40** 2563
[11] Hussey M J and Murray A J 2005 *J. Phys. B: At. Mol. Opt. Phys.* **38** 2965
[12] Avaldi L, Camilloni R and Stefani G 1990 *Phys. Rev.* A **41** 134
[13] Cavanagh S J and Lohmann B 1999 *J. Phys. B: At. Mol. Opt. Phys.* **32** L261
[14] Weigold E and McCarthy I E 1999 *Electron Momentum Spectroscopy* (New York: Kluwer /Plenum)
[15] Boudaiffa B *et al* 2000 *Science* **287** 1658
[16] Ptasinska S *et al* 2004 *J. Chem. Phys.* **120** 8505
[17] Colyer C J *et al* 2007 *New J. Phys.* **9** 41
[18] Varella M T D N *et al* 1999 *J. Chem. Phys.* **111** 6396
[19] Huels M A *et al* 1998 *J. Chem. Phys.* **108** 1309
[20] Denifl S *et al* 2003 *Chem. Phys. Lett.* **377** 74
[21] Hanel G *et al* 2003 *Phys. Rev. Lett.* **90** 188104
[22] Champion C 2003 *Phys. Med. Biol.* **48** 2147
[23] Champion C *et al* 2006 *Phys. Rev.* A **73** 012717
[24] Champion C, Hanssen J and Hervieux P A 2001 *Phys. Rev.* A **63** 052720
[25] Irvine W M *et al* 1989 *Astrophys. J.* **342** 871
[26] Gutowski M, Skurski P and Simons J 2000 *J. Am. Chem. Soc.* **122** 10159
[27] Pelc A *et al* 2002 *Chem. Phys. Lett.* **361** 277
[28] Pelc A *et al* 2003 *Vacuum* **70** 429
[29] Prabhudesai V S *et al* 2005 *Chem. Phys. Lett.* **405** 172
[30] Vizcaino V *et al* 2006 *New J. Phys.* **8** 85
[31] Allan M 2006 *J. Phys. B: At. Mol. Opt. Phys.* **39** 2939
[32] Bharathi S M *et al* 1990 *J. Electron Spectrosc. Relat. Phenom.* **53** 51
[33] Nixon K L *et al* 2008 *Chem. Phys. Lett.* **451** 18
[34] Nixon K L, Lawrance W D and Brunger M J 2009 *Chem. Phys. Lett.* **474** 23
[35] Lohmann B, Meng X-K and Keane M 1992 *J. Phys. B: At. Mol. Opt. Phys.* **25** 5223
[36] Gao J, Peacher J L and Madison D H 2005 *J. Chem. Phys.* **123** 204302
[37] Gao J, Madison D H and Peacher J L 2005 *J. Chem. Phys.* **123** 204314
[38] Gao J, Madison D H and Peacher J L 2006 *J. Phys. B: At. Mol. Opt. Phys.* **39** 1275
[39] Lee C, Yang W and Parr R G 1988 *Phys. Rev.* B **37** 785
[40] Guerra C F *et al* 1998 *Theor. Chem. Acc.* **99** 391
[41] Furness J B and McCarthy I E 1973 *J. Phys. B: At. Mol. Phys.* **6** 2280
[42] Perdew J P and Zunger A 1981 *Phys. Rev.* B **23** 5048
[43] Padial N T and Norcross D W 1984 *Phys. Rev.* A **29** 1742
[44] von Niessen W, Bieri G and Åsbrink L 1980 *J. Electron Spectrosc. Relat. Phenom.* **21** 175
[45] Ehrhardt H *et al* 1986 *Z. Phys.* D **1** 3
[46] Al-Hagan O *et al* 2009 *Nat. Phys.* **5** 59